AlCoCrFeNi high entropy alloy fabricated via selective laser melting reinforced by Fe-based metallic glass

Qi Jiang[a], Peilei Zhang[a,b*], Zhishui Yu[a], Yingtao Tian[c], Songyun Ma[d]

[a]School of Materials Engineering, Shanghai University of Engineering Science, Shanghai 201620, China

[b]Fraunhofer Institute for Laser Technology ILT, Aachen 52074, Germany

[c]Department of Engineering, Lancaster University, Lancaster LA1 4YW, United Kingdom

[d]Institute of General Mechanics, RWTH Aachen University, Aachen 52062, Germany

Abstract

The 5% Fe-based amorphous reinforced AlCoCrFeNi high-entropy alloy (HEA) specimens were prepared by selective laser melting (SLM) technique. The mixed of Fe-based amorphous reduces the grain diameter and eliminates the presence of texture. Meanwhile, the anisotropy of the specimen was reduced. The addition of Fe-based amorphous causes the precipitation of FCC phase in the body-centered cubic (BCC) matrix, and the face-centered cubic (FCC) phase is uniformly distributed at the grain boundaries. The presence of FCC phase significantly reduces the internal stress of the specimen. The elements in the amorphous alloy solidly dissolve into the BCC matrix during the printing process, further strengthening the BCC matrix. The residual amorphous and nanocrystalline phases also result in a significant improvement in the performance of the specimen.

Keywords: 3D printing, High-entropy alloys, Amorphous materials, Composite materials, Microstructure

1. Introduction

High-entropy alloys (HEAs) have attracted increasing attention due to their excellent mechanical,

* Corresponding authors.
E-mail addresses: peilei@sues.edu.cn (P. Zhang)

chemical, and physical properties [1]. However, the mechanical properties of the parts produced by conventional processing of the AlCoCrFeNi HEA are far below the standards for structural materials [2]. The selective laser melting (SLM) technology could produce fine grains with low segregation because of the large cooling rates. Meanwhile, the mechanical properties will be improved too [3]. In order to further strengthen the HEAs, some researchers have controlled the body-centered cubic (BCC) and face-centered cubic (FCC) phase transitions by changing the ratio of the constituent elements of HEAs [4]. Some researchers have enhanced the strength of HEAs by adding other elements, such as Si [5], B [6] and Nb [7] et al. However, these strengthening effects were not obvious, so in the study of Li et al. [8], an attempt was made to strengthen FeCoCrNiMn HEA using Fe metallic glass with almost the same matrix, and the maximum hardness of the specimen was finally obtained as 15.17 GPa. In this paper, based on previous studies on the strengthening of AlCoCrFeNi HEA by different elements. The exploratory experiments were conducted using the SLM technique with 5 wt% $(Fe_{0.76}B_{0.1}Si_{0.09}P_{0.05})_{99}Nb_1$ amorphous as the strengthening phase. The microstructure and micromechanical properties of the samples were studied respectively. The grain size of AlCoCrFeNi HEA, which mixed with amorphous is significantly reduced and the hardness is greatly increased. This study provides a new idea for strengthening AlCoCrFeNi HEA prepared by SLM.

2. Materials and Methods

The high purity (>99.99%) equimolar AlCoCrFeNi HEA powder and $(Fe_{0.76}B_{0.1}Si_{0.09}P_{0.05})_{99}Nb_1$ (at%) amorphous powder were employed as raw materials (Fig. 1(a)). The preset powder was placed in the ball mill tank in the ratio of 95wt% HEA and 5wt% amorphous, and ball milled for 1.5 hours with 150 rpm. The agate grinding balls were used to avoid pollution. The powder mixed by ball milling (Fig. 1(b)) was printed according to the SLM parameters shown in Table 1. The scanning strategy uses a 90° deflection per layer. The sample with the highest relative density was used to analysis the microstructure and hardness. The X-

Ray diffraction (XRD) and differential scanning calorimeter (DSC) was used to identify the phase composition in the specimen, and the electron back-scattered diffraction (EBSD) and scanning electron microscope (SEM) was used to further analyze the microstructure. The hardness of the specimen is obtained by nanoindentation. Berkovich indenter was used, accompanied by the pressure of 10mN and a full load time of 10s.

Table. 1. The SLM parameters for printing

Laser power P, (W)	Scanning speed v, (mm/s)	Hatching space h, (mm)	Layer thickness t, (mm)
90-230	1000-1700	0.095	0.025

3. Results and discussion

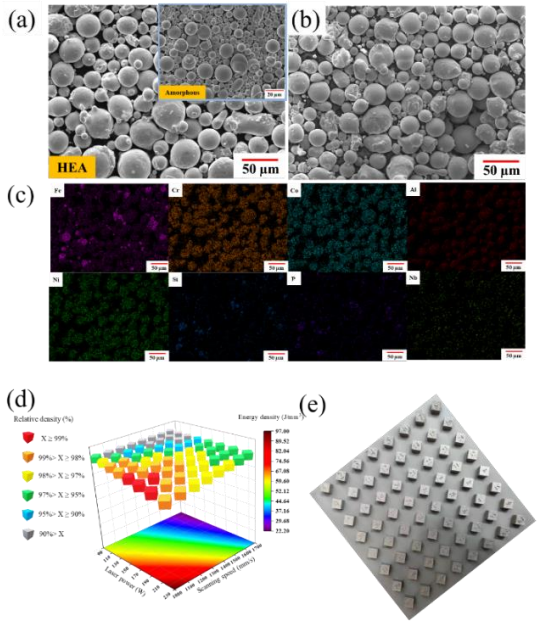

Fig. 1. (a) Particle morphology of HEA powder and amorphous alloy powder; (b) Particle morphology of mixed powder; (c) EDS element maps of mixed powder; (d) Relationship between energy density and relative densities for different process parameters; (e) Physical picture of specimen.

The mixed powder is uniformly distributed after ball milling treatment (As shown in Fig. 1(b) and (c)). The specimens are produced according to the parameter matrix shown in Fig. 1(d) (physical picture was

shown in Fig. 1 (e)). When the energy density (E) is greater than 71.58 J/mm^3 (where E=P/(vth)[9]), the densities of the specimens do not continue to increase but show a decreasing trend. Therefore, the samples with the energy density of 71.58J/mm^3 and relative density of 99.5% (Measured by Archimedes principle) will be analyzed in the following analysis.

In all views of the inverse pole figures (IPFs), the grain growth distribution of the specimen mixed with amorphous alloy is uniform and there is no tendency of epitaxial growth (Fig. 2(a)). The grain diameter statistics revealed that the addition of Fe-based amorphous grains limited the grain growth [8]. As shown in Fig. 2(a), the average grain diameter decreased from 3.42 μm (HEA) to 1.61 μm (HEA+Amorphous). The element of Si had been shown to have the effect of refining AlCoCrFeNi grains [5]. The element Nb has the same effect [7]. The intensity of 2.85 multiples of uniform density (mud) (Amorphous + HEA) was lower than that HEA alloy (11.71 mud) (Fig. 2(b) and Fig. 2(c)). The PFs of HEA showed a strong {100}<001> texture. The preferred growth direction of the BCC grains formed by printing HEA alloys is <001>, and the stronger texture intensity is easily formed in this direction [9]. The XRD results show that the print specimen mixed with amorphous alloy retains the BCC phase in the original powder and produces B2 and FCC phases (Fig. 2(d)). The increase of Fe element (mixed with Fe-amorphous alloy) can significantly increase the valence electron concentration (VEC), thus stabilizing the FCC phase and promoting the transition of the primary phase from the BCC phase to the FCC phase [4]. Small amounts of B element can form needle-like Cr-rich borides, which will act as nucleation sites for heterogeneous nucleation. The needle-like Cr-rich borides also promote the formation of the B2 phase [6]. As shown in Fig. 3(a), there was no significant elemental segregation in the sample. However, a point scan of the phases reveals that there was a little difference in the content of the element. Combined with our previous work[1], we can conclude that the white precipitated phase is the FCC phase. The local average misorientation (LAM)

angle of the HEA specimen is significantly larger than that of the mixed amorphous alloy specimen (Fig. 2(e)). The FCC phase precipitated at the grain boundaries of mixed amorphous alloy specimens can effectively reduce strain, dislocations, and lattice disorder[3].

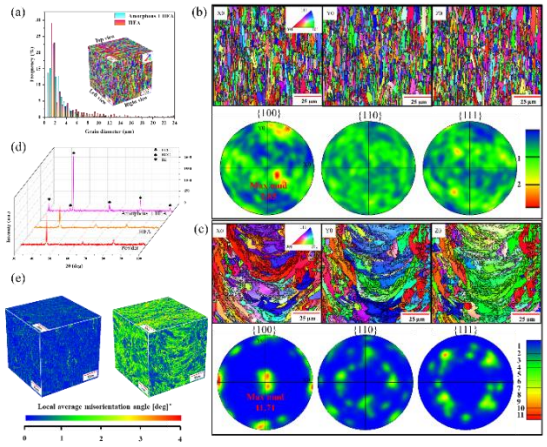

Fig. 2. (a) Comparison of grain diameter of HEA and amorphous+HEA specimens and IPF plots of amorphous+HEA specimens on three views; (b) IPF_X0, IPF_Y0, IPF_Z0 and PF plots of printed amorphous+HEA right view; (c) IPF_X0, IPF_Y0, IPF_Z0 and PF plots of printed HEA right view; (d) XRD patterns of amorphous+HEA specimens, HEA specimens and powders; (e) LAM of amorphous+HEA and HEA specimens on three views.

The mixed of amorphous alloy has significantly increased the hardness and elastic modulus of the specimens compared to that of AlCoCrFeNi [2]. As shown in Fig. 3(b-c), the maximum hardness and elastic modulus of the specimens are 18.01 GPa, 276.14 GPa (HEA+amorphous) and 14.721 GPa, 249.648 GPa (HEA), respectively. The DSC test results show that amorphous phase was also present in the sample (ΔH= -0.58 J/g). The edges of the indentation of FCC+BCC phase have a significant rebound due to the enhanced plasticity of the FCC phase in this region (Fig. 3(i)) [2]. However, the FCC phase also reduces the local hardness of the specimen. The microstructures at the locations of the indentations in Fig. 3(g) and (h) are similar, and both are BCC matrix phases. The difference in hardness can be seen according to Load-

displacement curves (Fig. 3(f)). Combined with the DSC test results (Fig. 3(d)), it could be inferred that there were nanoscale grains at the position in Fig. 3(g). Meanwhile, the nanoscale grains play a role in strengthening the matrix, and its elastic modulus value is much higher than the HEA used in this paper[10]. The main strengthening mechanisms for amorphous phases are fine grain strengthening and solid solution strengthening, while the amorphous and nanocrystalline phases were retained during the printing process are the main reasons for the significant increase in specimen hardness.

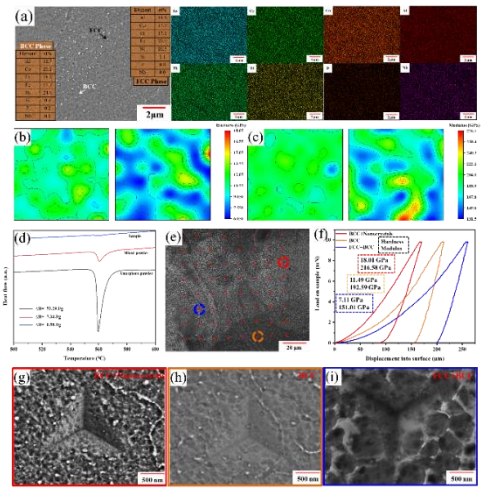

Fig. 3. (a) EDS element maps of sample; (b) Nano-hardness contour map(Left: HEA; Right: HEA+amorphous); (c) Elastic modulus contour map(Left: HEA; Right: HEA+amorphous); (d) DSC tests result on powder and mixed amorphous specimens; (e) Nanoindentation location distribution map; (f) Load-displacement curves on different phases; (g-i) The indentation shape corresponding to the curve shown in Fig. 3(f).

4. Conclusions

The strength of equimolar AlCoCrFeNi high-entropy alloy specimens produced by SLM was significantly enhanced by 5 wt% of Fe-based amorphous. The addition of Fe-based amorphous drives the precipitation of FCC phase from the primary BCC phase. Compared with the HEA sample, the average grain diameter decreased by 52.9%, and eliminates the {100}<001> texture. The hardness and elastic

modulus of the sample was enhanced by solid solution of the elements in the Fe-based amorphous with the HEA matrix, and the fine crystal strengthening is also the main strengthening concentration according to the Hall-Petch equation, while the residual amorphous and nanocrystalline phases further enhance the hardness of the specimen. The highest hardness and elastic modulus obtained were 18.01 GPa and 276.14 GPa, respectively.

Declaration of Competing Interest

None.

Acknowledgements

This research was supported by Natural Science Foundation of China (52075317).

References

[1] X. Wei, P. Zhang, Z. Yu, H. Yan, D. Wu, H. Shi, J. Chen, Q. Lu, Y. Tian, S. Ma, W. Lei, Effect of phase transformation on mechanical properties of Al16.80Co20.74Cr20.49Fe21.28Ni20.70 high entropy alloy coatings processed by laser cladding, J. Alloys Compd. 862 (2021). https://doi.org/10.1016/j.jallcom.2020.158563.

[2] G. Muthupandi, K.R. Lim, Y.S. Na, J. Park, D. Lee, H. Kim, S. Park, Y.S. Choi, Pile-up and sink-in nanoindentation behaviors in AlCoCrFeNi multi-phase high entropy alloy, Mater. Sci. Eng. A. 696 (2017) 146–154. https://doi.org/10.1016/j.msea.2017.04.045.

[3] C. Zhang, J. Zhu, C. Ji, Y. Guo, R. Fang, S. Mei, S. Liu, Laser powder bed fusion of high-entropy alloy particle-reinforced stainless steel with enhanced strength, ductility, and corrosion resistance, Mater. Des. 209 (2021) 109950. https://doi.org/10.1016/j.matdes.2021.109950.

[4] Q. Fan, C. Chen, C. Fan, Z. Liu, X. Cai, S. Lin, C. Yang, Effect of high Fe content on the microstructure, mechanical and corrosion properties of AlCoCrFeNi high-entropy alloy coatings

prepared by gas tungsten arc cladding, Surf. Coatings Technol. 418 (2021) 127242. https://doi.org/10.1016/j.surfcoat.2021.127242.

[5] H. Liu, S. Sun, T. Zhang, G. Zhang, H. Yang, J. Hao, Effect of Si addition on microstructure and wear behavior of AlCoCrFeNi high-entropy alloy coatings prepared by laser cladding, Surf. Coatings Technol. 405 (2021) 126522. https://doi.org/10.1016/j.surfcoat.2020.126522.

[6] V. Ferrari, W. Wolf, G. Zepon, F.G. Coury, M.J. Kaufman, C. Bolfarini, C.S. Kiminami, W.J. Botta, Effect of boron addition on the solidification sequence and microstructure of AlCoCrFeNi alloys, J. Alloys Compd. 775 (2019) 1235–1243. https://doi.org/10.1016/j.jallcom.2018.10.268.

[7] S.G. Ma, Y. Zhang, Effect of Nb addition on the microstructure and properties of AlCoCrFeNi high-entropy alloy, Mater. Sci. Eng. A. 532 (2012) 480–486. https://doi.org/10.1016/j.msea.2011.10.110.

[8] N. Li, S. Wu, D. Ouyang, J. Zhang, L. Liu, Fe-based metallic glass reinforced FeCoCrNiMn high entropy alloy through selective laser melting, J. Alloys Compd. 822 (2020) 153695. https://doi.org/10.1016/j.jallcom.2020.153695.

[9] B. Li, L. Zhang, Y. Xu, Z. Liu, B. Qian, F. Xuan, Selective laser melting of CoCrFeNiMn high entropy alloy powder modified with nano-TiN particles for additive manufacturing and strength enhancement: Process, particle behavior and effects, Powder Technol. 360 (2020) 509–521. https://doi.org/10.1016/j.powtec.2019.10.068.

[10] M. Ghanbariha, M. Farvizi, T. Ebadzadeh, A. Alizadeh Samiyan, Effect of ZrO2 particles on the nanomechanical properties and wear behavior of AlCoCrFeNi–ZrO2 high entropy alloy composites, Wear. 484–485 (2021) 204032. https://doi.org/10.1016/j.wear.2021.204032.